frontiers in Materials

ORIGINAL RESEARCH
published: 31 May 2021
doi: 10.3389/fmats.2021.670638

Dysprosium Oxide-Supported CaO for Thermochemical Energy Storage

Larissa Fedunik-Hofman[1,2], Alicia Bayon[2], Xiang Gao[3], Antonio Tricoli[3] and Scott W. Donne[1]**

[1] Discipline of Chemistry, The University of Newcastle, Callaghan, NSW, Australia, [2] CSIRO Energy, Newcastle, NSW, Australia, [3] College of Engineering and Computer Science, Australian National University, Canberra, ACT, Australia

A novel CaO-based material supported with $Ca_3Al_2O_6$ and Dy_2O_3 was found to show excellent performance as a thermochemical energy storage material for use in solar thermal power plants. It retains a carbonation conversion capacity of 82.7% for a period of 40 cycles, as well as exothermic heats of reaction of 582.2 kJ kg^{-1}, up to seven times greater than other materials found in the literature. The improved performance was attributed to the greater prevention of sintering and retention of high surface area by the addition of two inert supports: $Ca_3Al_2O_6$ and Dy_2O_3. Long-term effectiveness of the novel material was also evaluated by using a sintering model. It retains an energy storage utilization of 6.2 kg kWh^{-1} after 30 years of cycling, while commercial limestone would require 81 tons kWh^{-1} equivalent. Limestone requires replacement every six thermal cycles, making it impractical for real thermochemical energy storage implementation. The extra cost associated with the addition of supports in this CaO-based material is justified by the long-term durability, which would imply a reduction in the overall capital and operational expenditure of the plant.

Keywords: thermochemical energy storage, calcium looping, solar energy, concentrated solar thermal, Thermogravimetric analysis (TGA), differential scanning calorimetry

OPEN ACCESS

Edited by:
Vardan Galstyan, University of Brescia, Italy

Reviewed by:
Roberto Gonzalez Rodriguez, Texas Christian University, United States
Jong Hoon Joo, Chungbuk National University, South Korea

***Correspondence:**
Alicia Bayon
abayonsa@asu.edu
Scott W. Donne
scott.donne@newcastle.edu.au

Specialty section:
This article was submitted to Energy Materials, a section of the journal Frontiers in Materials

Received: *10 March 2021*
Accepted: *12 April 2021*
Published: *31 May 2021*

Citation:
Fedunik-Hofman L, Bayon A, Gao X, Tricoli A and Donne SW (2021) Dysprosium Oxide-Supported CaO for Thermochemical Energy Storage. Front. Mater. 8:670638. doi: 10.3389/fmats.2021.670638

INTRODUCTION

Renewable energy generation and storage systems are a key strategy in order to reduce CO_2 emissions and limit global warming (Greenblatt et al., 2017). CO_2 capture technologies are essential for transitioning into novel renewable energy-based society while still obtaining an economic return on the current infrastructure. However, CO_2 capture itself is not enough to solve the emissions problem. CO_2 capture technologies could be coupled with CO_2 storage, which solves in part the problem of taking carbon emissions out of the atmosphere. Thus, if instead of storing CO_2 we can utilize it effectively for other purposes, then there is a benefit (not only cost) on the carbon emissions. Nowadays, CO_2 is widely use in food industry for conservation. However, this CO_2 is not reused it in a way that it is easily storable and utilize.

Commercial concentrated solar power (CSP) plants employ sensible heat storage, and various candidate solar salts and other storage media have been explored (Gil et al., 2010; Liu M. et al., 2016). However, CSP plants require a higher levelized cost of electricity than other renewable alternatives, limiting deployment of these technologies (Starke et al., 2018; Awan et al., 2019). One of the main alternatives for cost reduction is replacing the low- efficiency subcritical Rankine cycle with the highly efficient supercritical CO_2 Brayton power cycle. Specifically, this power cycle has been demonstrated to achieve solar to electricity efficiencies as high as 55% when operating at

temperatures around 700°C (Calle et al., 2018). However, there are no commercially established energy storage systems for power cycles operating at such high temperatures. A promising alternative is the use of thermochemical energy storage (TCES) (André et al., 2016; Prieto et al., 2016; André and Abanades, 2018). The gas-solid reactions involved in TCES have high energy storage densities, making the process suitable for long-term energy storage (Bayon et al., 2018). Of all TCES technologies under investigation currently, carbonate looping has been found to have the greatest potential in the range of temperatures suitable for supercritical CO_2 Brayton cycles (Bayon et al., 2018).

The carbonate looping cycle based on $CaCO_3$ has been well researched for both TCES storage (Chacartegui et al., 2016; Prieto et al., 2016; Benitez-Guerrero et al., 2017, 2018; Ortiz et al., 2018a,b); and CO_2 capture technologies (Grasa et al., 2008; Erans et al., 2018). The calcination reaction is endothermic and can be driven by concentrated solar energy, as shown in Eq. (1), where ΔH_r is the reaction enthalpy (kJ mol^{-1}). The reaction products, CaO and CO_2, are stored separately. The reverse carbonation reaction recombines the calcination products in a separate reactor, releasing heat to be transferred to the gas turbine (Edwards and Materić, 2012); i.e.,

$$CaCO_3(s) \leftrightarrow CaO(s) + CO_2(g)\ (\Delta H_r(25^\circ C) = 178\ kJ\ mol^{-1}) \quad (1)$$

One of the major challenges associated with carbonate looping is the declining conversion efficiency of the carbonation reaction with ongoing thermal cycling. According to Grasa et al. (2008) carbonation conversion decreases dramatically during the first 20 cycles to a reversible conversion of about 8%. This results in a large proportion of inactive CaO cycling through the carbonate looping system, which leads to increased capital and operating costs (Edwards and Materić, 2012). At high calcination temperatures (>850°C), the decrease in the extent of conversion has been mainly attributed to the sintering of CaO grains (Benitez-Guerrero et al., 2017). The driving force for sintering is the reduction of surface energy of the grains caused by decreasing their surface area or increasing their grain size (Stone, 1960). Reducing the surface area reduces CaO reactivity by decreasing the amount of active sites available for the carbonation reaction (Liu W. et al., 2016), leading to longer CO_2 diffusion pathways.

High sintering resistance is related to the refractory nature of a material. Tammann temperature provides an indication for a material's susceptibility to sintering (Aihara et al., 2001). The correlation between Tammann (T_T) and melting temperatures (Tm) is described by the following relationship:

$$T_T = 0.5T_m \quad (2)$$

Hence, supporting materials with melting points higher than that of $CaCO_3$ (such as Dy_2O_3) will theoretically impart sintering-resistant properties to the sorbent (Liu et al., 2012b).

The onset of sintering is influenced by other factors in addition to the material's Tammann temperature, such as particle size and morphology, including the extent of porosity. For a discussion of the role of supports from a morphological perspective, see section "Characterization Results."

In order to improve carbonation efficiency and hence cyclability, the use of synthetic CaO-based materials synthesized with sintering-resistant inert supports is well documented (for CO_2 capture applications) (Liu et al., 2012b). A variety of materials have been investigated, such as $CaTiO_3$ (Liu et al., 2012b), Al_2O_3 (Broda et al., 2012), Y_2O_3 (Derevschikov et al., 2011), SiO_2 (Li et al., 2014; Sanchez-Jimenez et al., 2014), and oxides of Si, Co, Ti, Cr, Ce, and Zr (Lu et al., 2009). Synthesis processes usually involve dispersing CaO in a stable, solid matrix made up of the inert material, acting to preserve the available active surface layer of CaO and preventing loss of conversion with cycling (Li et al., 2005). Some of the most extensively investigated supports include aluminium-containing materials such as calcium aluminates, which form different polymorphs depending on the preparation method; e.g., mayenite ($Ca_{12}Al_{14}O_{33}$) (Li et al., 2005; Liu et al., 2012a), $Ca_9Al_6O_{18}$ (Zhou et al., 2012, 2013; Radfarnia and Sayari, 2015), or $Ca_3Al_2O_6$ (Angeli et al., 2014; Li et al., 2015; Sun et al., 2016; Wang et al., 2018). These supports have been found to be highly effective at stabilizing CaO, particularly when $Ca_3Al_2O_6$ is prepared using nitrate precursors (Zhou et al., 2012; Azimi et al., 2019). There is less research on the use of active supports as dopants for CaO-based sorbents. Active supports which have been examined include MgO (both dolomites and synthetically doped sorbents) (Albrecht et al., 2008; Liu et al., 2012a; Ping et al., 2016) and Li_2SO_4 (Lu and Wu, 2016).

Recently, lanthanides have become an attractive group of materials for use as supports. Several lanthanides have been tested as supports for CaO for CO_2 capture technologies, both active (able to absorb CO_2) (Cotton et al., 1999) and inactive (Luo et al., 2010). A CaO/La_2O_3 material produced using sol-gel combustion synthesis displayed good performance for 20 cycles under both inert gas and 100% CO_2 atmosphere (Luo et al., 2010). A CaO/La_2O_3 composite was also synthesized by Albrecht et al. (2008) using a hydrothermal process with nitrate precursors, limestone and tetrahydrofuran as a solvent. Materials containing small amounts of La_2O_3 showed a higher absorption capacity through 30 cycles than untreated limestone. However, this benefit was not retained with longer term cycling, with CO_2 capture capacity comparable to that of untreated limestone after 80 cycles (Albrecht et al., 2008).

Hu et al. (2015) incorporated Nd_2O_3 into CaO particles by wet mixing for CO_2 capture purposes. Improved durability and higher carbonation conversion were observed (67% after 100 cycles at a calcination temperature of 900°C), which was attributed to the prevention of sintering (Hu et al., 2015). Although the authors describe Nd_2O_3 as an inert solid sorbent, it is actually an effective CO_2 sorbent (Perry, 2015). Taking this into account and noting the drop off in conversion capacity at more severe calcination conditions, it is likely that the improved carbonation conversion is also due to the CO_2 uptake of Nd_2O_3 compared to inactive supports such as calcium aluminate. Hu et al. (2016) also supported CaO with Yb_2O_3, which achieved modest sintering-resistance (17% carbonation conversion after 50 cycles when tested under severe calcination conditions, a 9.5% improvement compared to CaO). However, the use of Pr_6O_{11} as

a support for CaO was unsuccessful, which was attributed to its very high molecular weight (Hu et al., 2016).

To address the challenge of finding a material that exhibits durability with thermal cycling under TCES conditions (high calcination temperature and 100% CO_2 atmosphere), this work proposed the use of Dy_2O_3 as a support to CaO. It is envisaged that the use of Dy_2O_3 will be beneficial due to its high melting temperature (∼2340°C), which predicts high sintering resistance (Liu et al., 2012b). This is supported by the improved performance of lanthanide-supported CaO in the literature (Luo et al., 2010; Hu et al., 2015, 2016).

The inert support mayenite ($Ca_{12}Al_{14}O_{32}$) has been consistently shown to prevent sintering, despite possessing a comparatively low Tammann temperature (Li et al., 2005; Liu et al., 2012a). This work also proposes a combination of Dy_2O_3 and $Ca_3Al_2O_6$ which obtains exceptional sintering resistance, improving the durability of CaO as compared with other explored supports with smaller amount of inactive material. A further long-term performance analysis reveals that the use of Dy_2O_3 and $Ca_3Al_2O_6$ could also be feasible compared with other TCES materials, as no replacement of the storage material is required during the typical lifetime of a CSP plant (commonly 30 years) (Liu M. et al., 2016).

EXPERIMENTAL

Materials Preparation

Pechini-synthesized CaO (denoted as P-CaO or P-$CaCO_3$ in its carbonate form) was prepared using the Pechini method, following the steps described in the literature (Jana et al., 2010). The reagents utilized were $Ca(NO_3)_2$ (Sigma-Aldrich; 99.0% purity), $Al(NO_3)_3$ (Sigma-Aldrich; 99.0% purity), dysprosium(III) nitrate hydrate ($Dy(NO_3)_3.xH_2O$); (Sigma-Aldrich; 99.9% purity), citric acid (CA; $C_6H_8O_7$; Sigma-Aldrich; 99.5% purity) and ethylene glycol (EG; $HOCH_2CH_2OH$; Sigma-Aldrich; 99.8% purity). The quantities of the reagents used are shown in **Table 1** as well as the nomenclature of the synthesized products. A precursor with a CA molar ratio of 1:5 and a CA to EG ratio of 3:2 were utilized.

Approximately 0.3 mol (57.4 g) of CA was added to 100 mL of distilled water (Milli-Q) and stirred at 70°C until dissolved totally. The metal precursors $Ca(NO_3)_2$ (11.8 g) and $Dy(NO_3)_3$ (1.3 g) were then added to the solution, which was stirred for 3 h before the temperature was increased to 90°C. EG (10 mL) was added and the resulting solution was further stirred at the same temperature to remove the excess solvent until the solution became a viscous resin. The obtained resin was subsequently dried in an oven at 180°C for 5 h. The sample was then ground with an agate mortar to achieve fine particles and then calcined in a tube furnace. The furnace was programmed to 400°C for 2 h, before heating to 900°C at a ramp speed of 10°C min^{-1}, holding for 4 h and cooling to ambient temperature at 10°C min^{-1}. After calcination, the sample was ground again to ensure very fine particles were obtained.

To produce a material supported with both dysprosium oxide and calcium aluminate, the stoichiometry of the reaction of Al_2O_3 and CaO at high temperatures was analyzed. Several studies describe the production of the calcium aluminate known as mayenite; i.e.,

$$7Al_2O_3 + 12CaO \rightarrow Ca_{12}Al_{14}O_{33} \quad (3)$$

At temperatures greater than 850°C, mayenite can react with excess CaO to form tricalcium aluminate (Peng et al., 2015); i.e.,

$$Ca_{12}Al_{14}O_{33} + 9CaO \rightarrow 7Ca_3A_{12}O_6 \quad (4)$$

The stoichiometry of these reactions were used to estimate the amount of inert support in the material, and the amount of active CO_2 sorbent was determined based on the percentage of calcination conversion compared to the theoretical mass loss of 43.97% for $CaCO_3$ (see **Table 1**). It was assumed that there would be no reaction between the $Al(NO_3)_3$ and the $Dy(NO_3)_3$. For comparative purposes, materials composed only of Dy_2O_3, CaO, and CaO supported with calcium aluminate were also prepared (see **Table 1**).

TABLE 1 | Quantities of reagents used and characteristics of resulting powder samples.

Name	Precursor composition	CA (g)	EG (mL)	$Ca(NO_3)_2$ (g)	$Dy(NO_3)_3$ (g)	$Al(NO_3)_3$ (g)	CaO Yield (%)
P-Dy_2O_3	$Dy(NO_3)_3$	6.4	1.3	–	4.67	–	0
P-CaO	$Ca(NO_3)_2$	48.0	9.2	11.8	–	–	100
P-CaO-Al20	80 mol% $Ca(NO_3)_2$ 20 mol% $Al(NO_3)_3$	34.6	7.5	7.6	–	3.0	65
P-CaDy20	93 mol% $Ca(NO_3)_2$ 7 mol% $Dy(NO_3)_3$	51.6	10.0	11.8	1.3	–	88
P-CaDy-Al5	88.84 mol% $Ca(NO_3)_2$ 6.64 mol% $Dy(NO_3)_3$ 5 mol% $Al(NO_3)_3$	54.4	10.5	11.8	1.3	1.1	85
P-CaDy-Al10	83.71 mol% $Ca(NO_3)_2$ 6.29 mol% $Dy(NO_3)_3$ 10 mol% $Al(NO_3)_3$	57.4	11.1	11.8	1.3	2.2	81
P-CaDy-Al20	74.41 mol% $Ca(NO_3)_2$ 5.59 mol% $Dy(NO_3)_3$ 20 mol% $Al(NO_3)_3$	64.6	12.5	11.8	1.3	5.0	62

Material Characterization

Powder X-ray diffraction (XRD) analysis was performed using CuK_α radiation ($K_{\alpha 1}$ = 1.540598 Å; $K_{\alpha 2}$ = 1.544426 Å) at a scanning rate of 2.5° min^{-1} (step size = 0.026°, time per step = 0.31 s) over the 2θ range 15–70°. Diffraction patterns were analyzed with Joint Committee on Powder Diffraction Standards (JCPDS). Crystallite sizes were obtained using the Scherrer calculator function in PANalytical X'Pert HighScore software (Degen et al., 2014). The crystallite sizes were calculated using the peak at 37.4° (the most intense peak at 29° was not evaluated due to an overlap with the peak of Dy_2O_3) using:

$$d = \frac{0.89\lambda}{B\cos(\theta)} \quad (5)$$

where d is the mean crystallite diameter (Å), λ is the X-ray wavelength (Å), 0.89 is the shape factor for CaO, and B is the full width half maximum (FWHM) of the CaO diffraction peak (rad), taking into account instrumental peak broadening.

BET surface area, pore volume and pore size distribution were determined by N_2 adsorption-desorption analysis using a Micromeritics TriStar II 3020 surface area analyzer. All samples were degassed under vacuum for 4 h at 120°C prior to the measurement. Surface area was determined by applying the multipoint BET method, and isotherms were typically analyzed over the relative pressure range of 0.05–0.30. Pore volume and pore size distribution were determined using the BJH adsorption method.

SEM images were recorded by using a Zeiss Sigma VP FESEM. Samples were carbon coated before analysis. Energy dispersive spectroscopy (EDS) mapping was carried out using a Bruker light element SSD EDS detector. TEM images were recorded using a JEOL JEM-1200EXII TEM with STEM and EDS system. Samples were suspended in acetone, sonicated and dispersed on copper grids prior to analysis.

Calcination-Carbonation Cycling Analysis

The extent of conversion with cycling was monitored by thermogravimetric analysis (TGA) using a SETSYS Evolution 1750 TGA-DSC from SETARAM Instrumentation. Testing conditions varied based on calcination atmosphere (N_2/CO_2) and carbonation atmosphere (mixture of CO_2 and N_2/100% CO_2) (cf., **Table 2**). Experiments in the literature are typically carried out with calcination in N_2 and carbonation under a mixed atmosphere, so these conditions were replicated for comparative purposes. However, a CO_2 atmosphere is potentially more favorable, as using pure CO_2 as the reactor unit atmosphere avoids the need for multiple gas storage, separation and purification units, lowering costs and preventing compression losses (Schaube et al., 2011).

In a typical experiment under 100% CO_2, 18 mg of powder sample was placed into a 100 μL alumina crucible and subjected to 40 cycles of heating to 1000°C and subsequent cooling to 850°C (10°C min^{-1} heating rate), where the sample was held isothermally for 30 min to allow for carbonation. A constant CO_2 gas flow of 20 mL min^{-1} was utilized. Experiments such as these with calcination temperatures greater than 900°C are described as "severe" conditions. For an experiment with N_2 as the calcination atmosphere (described as "mild" calcination conditions), the sample was heated to 800°C, held isothermally for 10 min and then cooled to 650°C. The reacting gas was switched to a mixture of 75% v/v N_2 and 25% CO_2 and held isothermally for 30 min to allow for carbonation. The gas was then switched back to N_2 and cycling continued for 40 cycles.

TABLE 2 | Testing conditions and selected results for synthesized materials.

Sample	Calcination			Carbonation							References
	Temperature	Atmosphere	Time	Temperature	Pco2	Time	X(t) (% at cycle)				
	(°C)		(min)	(°C)	(% v/v)	(min)	1	20	40	100	
Severe Conditions											
P-CaDy20-CO_2	1000	CO_2	None	850	100	30	94.9	51.6	31.6		This work
P-CaDy-A120-CO_2	1000	CO_2	None	850	100	30	91.1	84.6	82.7		This work
P-CaDy-A110-CO_2	1000	CO_2	None	850	100	30	90.2	82.1	63.3		This work
P-CaDy-A15-CO_2	1000	CO_2	None	850	100	30	95.0	67.6			This work
P-CaO-A120-CO_2	1000	CO_2	None	850	100	30	88.8	80.2	72.8		This work
CalOLa-950	950	CO_2	10	650	25	15	85.5	36.0			Luo et al., 2010
Ca70Nd-1000	1000	N_2	5	650	15	15	99.1	48.9	29.1	15.1	Hu et al., 2015
Mild Conditions											
P-CaDy-A120-N2	800	N_2	10	650	25	30	100.0	87.5	76.0		This work
Ca70Nd-800	800	N_2	5	650	15	15	99.2	98.7	97.9	91.6	Hu et al., 2015
CalOYb-800	800	N_2	5	650	30	25	75.0	64.8			Hu et al., 2016
CalOLa-850	850	N_2	10	650	25	15	65.2	43.1			Luo et al., 2010
Ca70Nd-900	900	N_2	5	650	15	15	99.2	98.7	86.4	66.9	Hu et al., 2015
CalOYb-900	900	N_2	5	650	15	25	50.1	36.2	17.1		Hu et al., 2016

The carbonation conversion of CaO to $CaCO_3$ was calculated using:

$$X(t) = \left(\frac{m(t) - m_i}{X.m_{x=1}}\right)\left(\frac{M_{caco_3}}{M_{caco_3} - M_{cao}}\right) \quad (6)$$

where X(t) is the carbonation conversion extent as a function of time, m(t) is the mass of the sample (g) after time t (min) at the carbonation temperature or under the carbonation atmosphere (t = 30 min), m_i is the initial mass of the sample before carbonation (g), x is the active mass fraction of CaO, $m_{X\ =\ 1}$ is the theoretical mass of the sample in grams after 100% carbonation conversion (g; 43.97% mass gain) and M is the molar mass (g mol^{-1}).

As a means of comparing synthetic materials with different proportions of active material, effective carbonation conversion was calculated. The effective carbonation conversion, $X(t)_{eff}$, takes into account the inert portion of the material and was calculated as follows:

$$X(t)_{eff} = x.X(t) = \left(\frac{m(t) - m_i}{m_{x=1}}\right)\left(\frac{M_{caco_3}}{M_{caco_3} - M_{cao}}\right) \quad (7)$$

For ease of reference, X(t) refers to the "original (carbonation) conversion" and $X(t)_{eff}$ as "effective (carbonation) conversion" and a comparison of both properties is detailed in the results.

Differential scanning calorimetry was used to determine endothermic and exothermic heats of reaction. Cycling experiments under severe experimental conditions were used to obtain heats of reaction. SETARAM post-processing analysis software was used to integrate the heat flow peaks using the Bezier integration function.

Sintering Model

It has been noted that the practical use of modified synthetic TCES materials will depend on their economic performance, and the impact of inert supports on cost performance has yet to be evaluated in many studies (Valverde, 2013). Prices of inert supports are much higher than natural limestone (Qin et al., 2014), so the improvement in performance of the synthetic TCES materials must be quantified to justify their additional cost. The deactivation of the natural limestone occurs rapidly, which will require a replacement of the materials after a small number of thermal cycles (Grasa and Abanades, 2006). Deactivation of natural limestone was evaluated from cycling experiments performed by Sarrión et al. (2018) using limestone under realistic TCES conditions.

To determine the deactivation of the material with long-term cycling (i.e., assuming the same material is used during the whole lifetime of a CSP plant), the sintering model described by Grasa and Abanades (2006) was used to determine the carbonation conversion (X(N)) after N cycles. The decay trend could be correlated using the parameters deactivation constant (k), residual conversion (X_r) and N; i.e.,

$$X(N) = X_r + \frac{1}{\frac{1}{1-X_r} + KN} \quad (8)$$

This was used to model loss in conversion for P-CaO and P-CaDy-Al20 (see section "Feasibility Study" and **Table 1** for sample composition). The parameters k and X_r were determined using least squares regression. When this model proved unsuitable for modeling sintering over the first 40 cycles (as in the case of P-CaO-Al20 and limestone, referred to as Comm-$CaCO_3$), a semi-empirical model from Valverde et al. (2017) was used to determine the number of sorbent replacements required over the whole life of a CSP plant [assumed to be 30 years (Steinhagen and Nitsch, 2005)]; i.e.,

$$X(N) = X_r + \frac{X_1}{K(N-1) + \left(1 - \frac{X_r}{X_1}\right)^{-1}} \quad (9)$$

where X_1 is the carbonation conversion after the first cycle. In this model it is assumed that the material will be charged and discharged once a day and therefore the number of cycles is identical to the number of days of operation. For reference, it is assumed than replacement will be made when the conversion falls below 20%.

The mass specific storage utilization (kg kWh^{-1}) was evaluated using the experimentally determined exothermic heat of reaction of the candidate materials. To determine the required amount of material over the plant lifetime ($\mu_{Storage}$), the storage utilization after 30 years was obtained by dividing the number of material replacements ($R_{30\ years}$) by the heat storage capacity after 40 cycles as per:

$$\mu_{Storage} = \frac{R_{30\ years}}{\Delta H_r} \quad (10)$$

RESULTS AND DISCUSSION

Thermal Cycling and Initial Characterization

Table 2 sets out the experimental conditions and cycling results of synthesized oxides from this work and experiments from published literature. In order to examine the TCES potential, calcination and carbonation conversions were recorded up to 40 cycles (see **Table 2**). The thermal cycling results under two distinct experimental conditions, severe calcination and mild calcination, are discussed in sections "Cycling Under Severe Calcination Conditions" and "Cycling Under Mild Calcination Conditions," respectively.

As-synthesized materials were first characterized by XRD, as shown in **Figure 1**. In addition to peaks of Dy_2O_3, CaO and $Ca_3Al_2O_6$, the Dy-supported materials show peaks of calcium oxide minerals such as portlandite ($Ca(OH)_2$) and vaterite (a polymorph of $CaCO_3$). This indicates that these substances are not completely decomposed during the initial calcination process. Another possibility is that these compounds are formed due to materials reacting with atmospheric moisture and CO_2 post-calcination. Scans taken after cycling (**Figure 2**) indicate that both portlandite and vaterite decompose during the calcination process, while calcite ($CaCO_3$) forms during carbonation. Dysprosium carbonate was not detected in the scan, which shows that the dysprosium oxide does not undergo cycling to dysprosium carbonate.

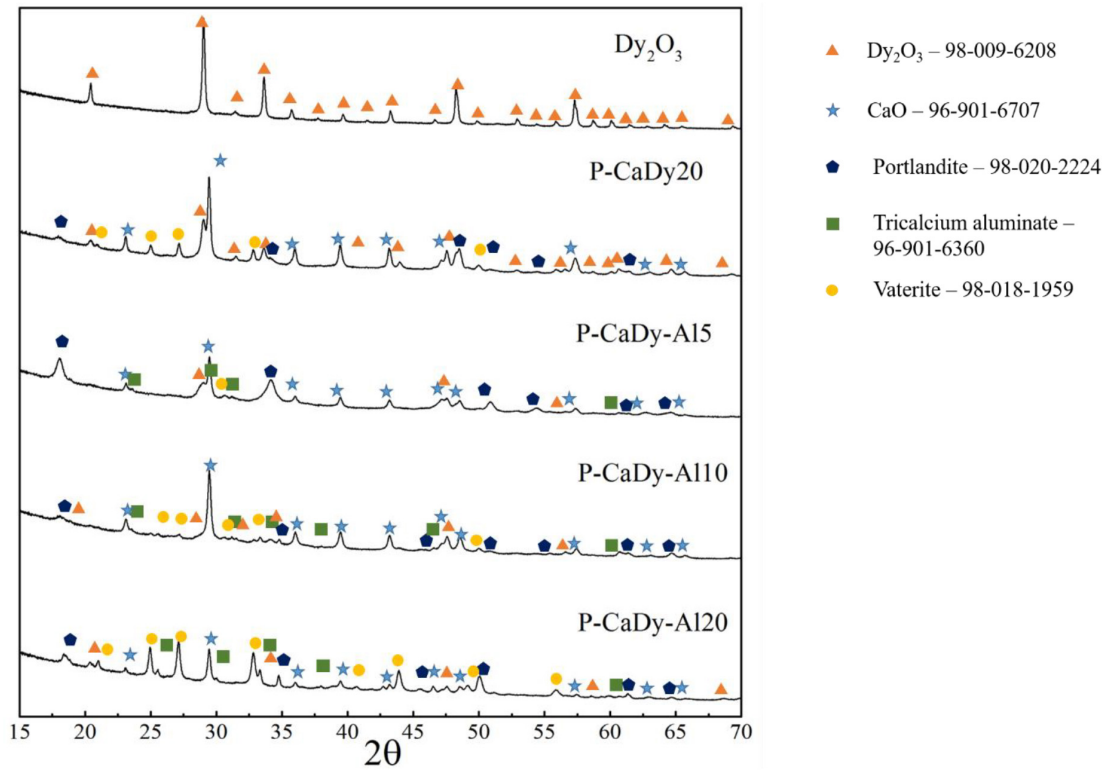

FIGURE 1 | XRD patterns of the as-synthesized materials.

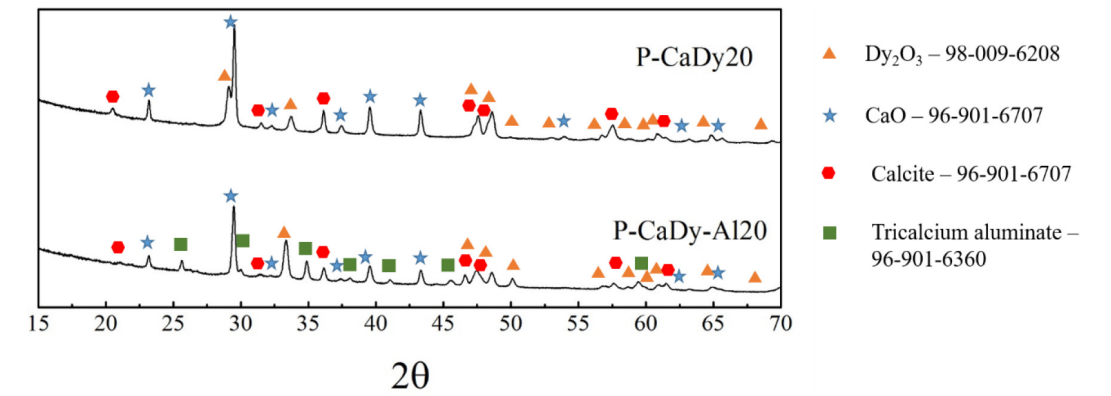

FIGURE 2 | XRD patterns of selected materials post TGA cycling.

Cycling Under Severe Calcination Conditions

To evaluate the TCES potential, the materials are cycled under severe calcination conditions (100% CO_2, cycling between 1000 and 850°C). The selected conditions, original conversion and reaction times are gathered in **Table 2**. The evolution with cycling of original and effective conversion are plotted in **Figures 3A,B**, respectively. The literature materials selected for comparison are Ca10La-950 (10% La_2O_3, calcined to 950°C) and Ca70Nd-1000 (70% Nd_2O_3, calcined to 1000°C).

When comparing the original conversion (**Figure 3A** and **Table 2**), it can be observed that the P-CaDy20-CO_2 suffers from a loss of conversion from 94.9% in the first cycle to 51.6% in cycle 20. It is important to note that this material has been synthesized without the addition of $Ca_3Al_2O_6$. When $Ca_3Al_2O_6$ is added, the material stability with cycling improves considerably. Addition of 5, 10 or 20% of the Al precursor results in an increase in conversion of 67.6, 82.1, and 84.6%, respectively, after 20 cycles. The latter two materials were cycled for a longer period, with the result that the material with a larger amount

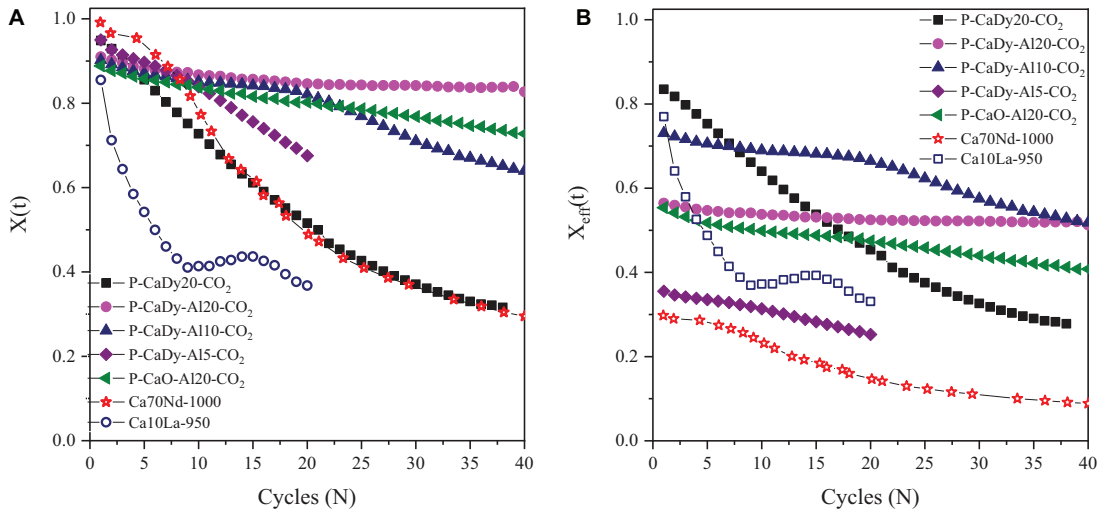

FIGURE 3 | Carbonation conversion compared to literature results – severe calcination conditions, **(A)** original carbonation conversion and **(B)** effective carbonation conversion. Empty symbols are literature.

of $Ca_3Al_2O_6$ (P-CaDy-Al20-CO_2) achieves the best stability in this study. This material also achieves the lowest decline in carbonation conversion with thermal cycling, with a decrease of only 8.3% after 40 cycles. The incorporation of Dy_2O_3 was further evaluated by comparing P-CaDy-Al20-CO_2 with P-CaO-Al20-CO_2 (synthesized without the Dy_2O_3 support). The latter shows a loss of conversion from 88.8% in the first cycle to 72.8% in cycle 40, although loss of conversion capacity is less extreme than the material synthesized with only Dy_2O_3 (P-CaDy20-CO_2). The stability of the synthesized materials can be classified in the following order:

> P-CaDy-Al20-CO_2 > P-CaO-Al20-CO_2 > P-CaDy-Al10-CO_2 > P-CaDy20-CO_2.

The materials selected for comparison from literature have the following Ca70Nd-1000 (70% Nd_2O_3, calcined to 1000°C) and Ca10La-950 (10% La_2O_3, calcined to 950°C) (see **Table 2**). The carbonation conversion achieved by P-CaDy20-CO_2 is higher at 20 and 40 cycles (15.6% and 2.7% higher than Ca10La-950 and Ca70Nd-1000, respectively). It is also necessary to highlight that the amount of inert support contained in Ca70Nd-1000 is much larger as compared to P-CaDy20-CO_2, and the latter slightly improved the carbonation conversion. When CaO was combined with both Dy_2O_3 and $Ca_3Al_2O_6$ (in P-CaDy-Al20-CO_2) the conversion is 48.6% and 35.7% higher after 20 cycles as compared to Ca10La-950 and Ca70Nd-1000, even though P-CaDy-Al20-CO_2 is calcined under more severe calcination conditions (higher temperature or CO_2 concentration). These results reveal that firstly, the use of Dy_2O_3 improves the stability of CaO, as compared with the supports La_2O_3 and Nb_2O_3, and secondly, that the extra addition of $Ca_3Al_2O_6$ significantly contributes to an increase in stability with cycle number.

To study the effect of the mass fraction of inert supports, the effective carbonation conversion is shown in **Figure 3B**. After 40 cycles P-CaDy-Al10-CO_2 and P-CaDy-Al20-CO_2 outperform all the materials in this study, as well as in the literature references. When 10% aluminium precursor is added (P-CaDy-Al10-CO_2), the effective carbonation conversion drops from 66.5% in cycle 20 to 51.8% in cycle 40, and the slope of the conversion decay indicates that the carbonation conversion is not yet stabilized after 40 cycles. However, the addition of 20% aluminium precursor (P-CaDy-Al20-CO_2) helps to maintain the effective carbonation conversion from 56.4% in cycle 1 to 51.3% in cycle 40. The best performing material P-CaDy-Al20-CO_2 has stabilized after 40 cycles with 82.7% original and 51.3% effective conversion capacities (see **Figures 3A,B**, respectively). In comparison, the Nd_2O_3 and La_2O_3 supported materials from the literature show much lower effective carbonation conversions after 40 cycles. Comparing effective carbonation conversion gives a more realistic picture of material performance, particularly in the case of Ca70Nd-1000, which contains 70% inert material. Additionally, only the Ca10La-950 is tested under 100% CO_2, while Ca70Nd-1000 is calcined under a N_2 atmosphere (see **Table 2**). Testing under pure CO_2 displaces the reaction equilibrium point to higher temperatures and is known to accelerate sintering and loss of conversion (Stanmore and Gilot, 2005). Therefore, the higher carbonation conversions of the materials in this work are particularly noteworthy, considering that the experimental conditions are more severe than those in the literature. Good performance under 100% CO_2 is also highly relevant to TCES, as these more realistically represent reactor conditions (Schaube et al., 2011).

Cycling Under Mild Calcination Conditions

To further evaluate the materials and compare with literature, the synthesized material which performed best under severe conditions (P-CaDy-Al20; cf., section "Cycling Under Severe Calcination Conditions") was tested under mild calcination conditions (100% N_2 calcination, 75:25 N_2:CO_2 carbonation, cycling between 800 and 650°C). As for section "Cycling Under

Severe Calcination Conditions," the selected conditions, original conversion and reaction times are gathered in **Table 2**, while original and effective carbonation conversion are plotted in **Figures 4A,B**, respectively. The literature materials selected for comparison are Ca70Nd-800/900 (70% Nd_2O_3, calcined to 800/900°C), Ca10Yb-800/900 (10% Yb_2O_3, calcined to 800/900°C), and Ca10La-850 (10% La_2O_3, calcined to 850°C).

When examining the original conversion (**Figure 4A**) it can be observed that the P-CaDy-Al20-N_2 achieves ∼100% carbonation conversion in the first cycle, dropping to 76% in cycle 40. Taking into account the fraction of inert support (**Figure 4B**), P-CaDy-Al20-N_2 achieves 62% carbonation conversion in the first cycle, and this drops to 55% carbonation conversion in cycle 40.

Compared to P-CaDy-Al20-CO_2 (**Figures 3A,B**) the carbonation conversion of P-CaDy-Al20-N_2 is initially greater, but this drops off with cycling and the material does not reach stable conversion after 40 cycles (**Figures 4A,B**). This could be due to the phenomenon of "self-reactivation" under CO_2 as compared to calcination under N_2 (Manovic and Anthony, 2005). It is well known that calcining CaO under 100% CO_2 displaces the reaction point to higher temperatures, and is known to accelerate sintering and loss of conversion (Stanmore and Gilot, 2005). Thermal cycling causes the development of a hard inward skeleton of low porosity, less reactive CaO, surrounded by a softer layer of reactive, porous CaO. This hard skeleton is hypothesized to keep the pore structure stable during cycling while the external soft skeleton is regenerated in each re-carbonation (Manovic and Anthony, 2005). The residual CO_2 uptake capacity was determined by the CaO skeleton structure, which is heavily influenced by the calcination temperature (Kierzkowska et al., 2013). Manovic and Anthony found that pre-treatment of limestone to temperatures greater than 1000°C increased residual conversion (Manovic and Anthony, 2005), which is reflected in this study.

P-CaDy-Al20-N_2 was then compared with materials from literature experiments. As shown in **Figure 4A**, P-CaDy-Al20-N_2 outperforms the La_2O_3 and Yb_2O_3 supported materials, but falls short of the Nd_2O_3 supported material. When considering effective carbonation conversion (**Figure 4B**), P-CaDy-Al20-N_2 clearly outperforms the Nd_2O_3-supported sample, which is predominantly composed of inert material (70%). It also outperforms the La_2O_3 supported material and is predicted to outperform the Yb_2O_3-supported material, which shows poor stability. P-CaDy-Al20 is therefore seen to perform well and exhibit high performance under both mild and severe experimental conditions. Its performance is best under 100% CO_2, conditions which are most relevant for TCES.

Characterization Results

Table 3 presents the crystallite sizes of the synthesized materials obtained using the Scherrer equation. Crystallite sizes range from 58 to 90 nm in the materials in their as-synthesized state. Using XRD results, similar crystallite sizes were initially obtained for P-CaDy20 and the supported material P-CaDy-Al20 (87 and 83 nm, respectively). However, a significant difference in the crystallite sizes is calculated after 40 calcination and carbonation cycles. Average crystallite size increases to 201 nm for P-CaDy20, while P-CaDy-Al20 reaches 128 nm after 40 cycles, which reflects its resistance to sintering.

Table 4 shows the results of BET and pore size analysis for the materials, as synthesized and after 40 cycles of calcination and carbonation cycling. Measurements show that supporting CaO with Dy_2O_3 results in a significant improvement in the retention of surface area. P-CaDy-Al20-c shows a reduction of surface area of only 3.4 $m^2\ g^{-1}$, as compared to P-CaO, which has almost negligible surface area after 40 cycles.

SEM images (**Figure 5**) show that the synthesized materials P-CaDy20 and P-CaDy-Al20 display a porous structure, indicative of high surface area. The morphology of Dy_2O_3 is seen to be more jagged. In **Figures 5a,b** it can be seen that the P-CaDy20 sinters significantly after 20 cycles. **Figure 5b** shows that the material clumps together, losing its fluffy, porous nature and develops rounded particle edges. However, with the

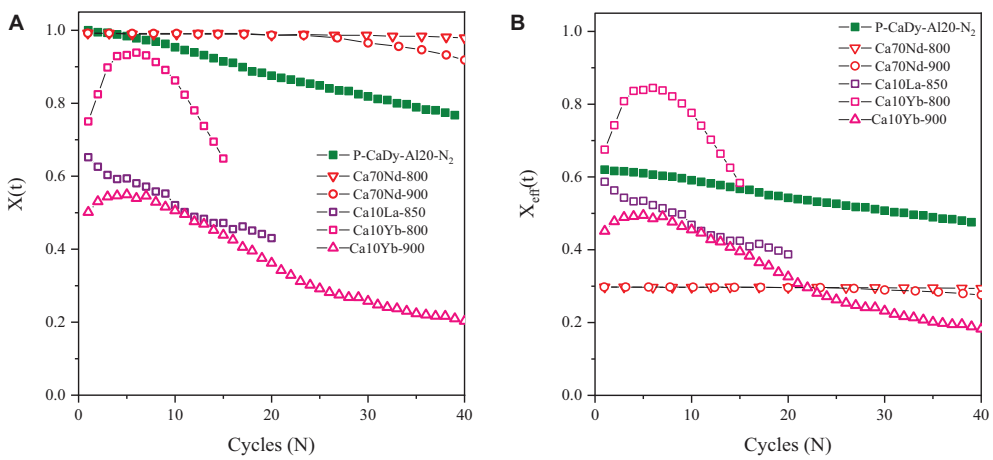

FIGURE 4 | Carbonation conversion compared to literature results – mild calcination conditions, **(A)** original carbonation conversion and **(B)** effective carbonation conversion. Empty symbols are literature.

TABLE 3 | Heat of reactions for TCES materials in this work and literature.

Material	Heat of reaction (kJ kg^{-1}; cycle)		References
	Endothermic	Exothermic	
P-CaO	413.8 (40)	229.5 (40)	This work
P-CaO-Al20	678.0 (40)	462.8 (40)	This work
P-CaDy-Al20	689.8 (40)	582.2 (40)	This work
$CaCO_3$ (limestone)	81.2 (40)*	NA	Sarrión et al., 2018
Co_3O_4	600.8 (1)	495.57 (1)	Carrillo et al., 2014
BaO_2	77 (1)	NA	Fahim and Ford, 1983
CuO	811** (0)	NA	Alonso et al., 2015
Mn_2O_3	161.8 (1)	79.3 (1)	Carrillo et al., 2014
$(Mn_{0.1}Fe_{0.9})_2O_3$	178.0 (1)	111.0 (1)	Carrillo et al., 2015
$(Mn_{0.33}Fe_{0.67})_2O_3$	199.60 (1)	177.8 (10)	Al-Shankiti et al., 2019; Hamidi et al., 2019
$(Co_{0.867}Fe_{0.133})_3O_4$	433.3 (1)	414.9 (1)	Block et al., 2014
$(Co_{0.99}Mn_{0.01})_3O_4$	490.8 (1)	424.8 (1)	Carrillo et al., 2014

**Value obtained from HSC Chemistry 8 ® and deactivation model.*
NA, not available.
***Denotes value has been obtained from database and not experimentally.*

TABLE 4 | Crystallite sizes of synthesized sorbents (as synthesized, at 30°C).

Material	Crystallite size (nm)
P-Dy_2O_3	108
P-CaDy20	70.8
P-CaDy-Al5	90.3
P-CaDy-Al10	57.8
P-CaDy-Al20	79.0

addition of an alumina support in P-CaDy-Al20, less sintering is evident (**Figures 5c,d**). The TEM images show the increased porosity of P-CaDy-Al20 (**Figures 6d–f**) compared to P-CaDy20 (**Figures 6a–c**). Note the dark regions in these figures which indicate the presence of Dy_2O_3.

Figure 7 displays EDS mapping for the as-synthesized materials, unsupported (P-CaDy20; **Figures 7A,C**) and supported (P-CaDy-Al20; **Figures 7B,D**). **Figure 7A** shows that the elements of P-CaDy20 are unevenly distributed across the material, particularly dysprosium. However, **Figure 7B** shows a much more thorough homogeneous distribution. In particular, the red dysprosium is barely visible due to complete overlap with the green calcium, which reflects the even dispersion of Dy_2O_3 across the CaO. Particle growth after cycling can be compared between the supported and unsupported materials. **Figure 7C** shows that P-CaDy20 exhibits significant particle growth after 40 cycles, while P-CaDy-Al20 resists sintering (**Figure 7D**).

Theories on how inert supports act to prevent sintering include the grain boundary "pinning effect" and the effect of densification. Adhesion of the support particle to the grain boundary was postulated to exert a pinning effect and hence provide a drag force to oppose grain growth (Li et al., 2013). Only the support particles on the grain boundaries will exert a pinning force. In this way, the support particles act as a "metal skeleton" – spacers to separate the $CaO/CaCO_3$ particles (Hu et al., 2015). Alternatively, inert spacers are suggested to suppress densification and loss of micro- or meso-porosity during repeated calcinations (Zhao et al., 2014). As $CaCO_3$ has a lower density than CaO, this leads to pore closure of unreacted CaO and increased diffusional resistance of CO_2. If CaO is supported with

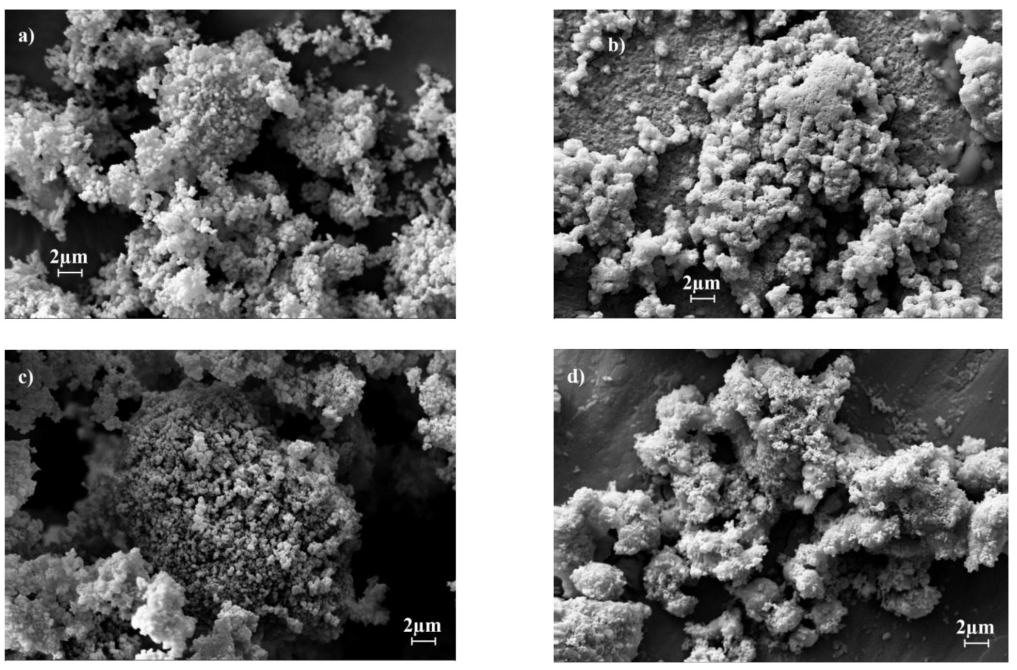

FIGURE 5 | SEM images for **(a)** P-CaDy20 as synthesized, **(b)** after 20 cycles, **(c)** P-CaDy-Al20 as synthesized, **(d)** after 20 cycles.

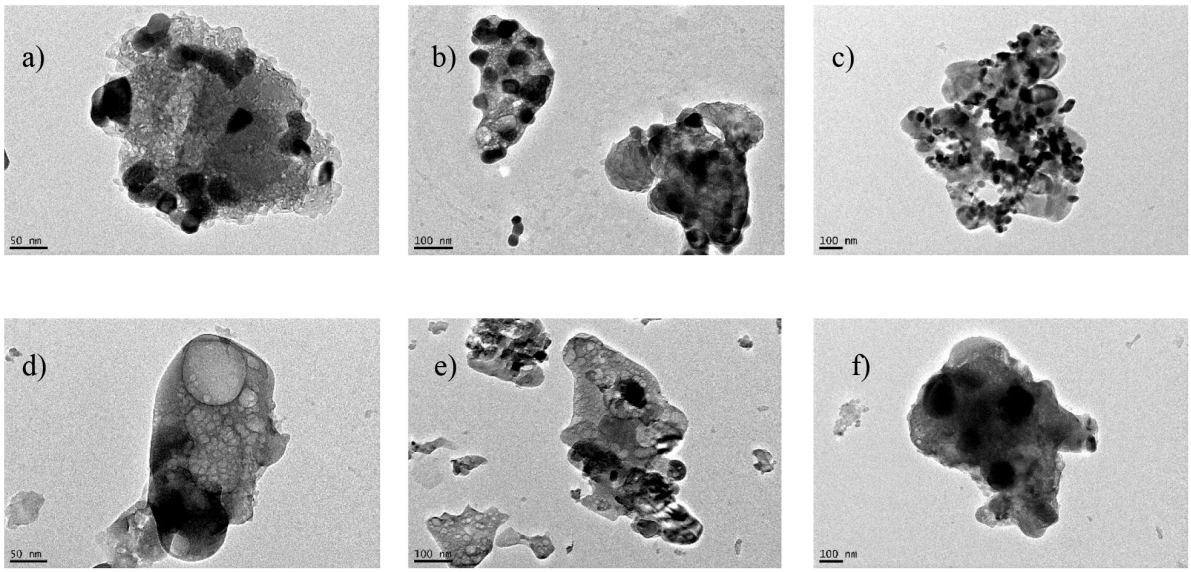

FIGURE 6 | TEM images for **(a)** and **(b)** P-CaDy20 as synthesized, **(c)** after 20 cycles, **(d)** and **(e)** PCaDy-Al20 as synthesized, **(f)** after 20 cycles.

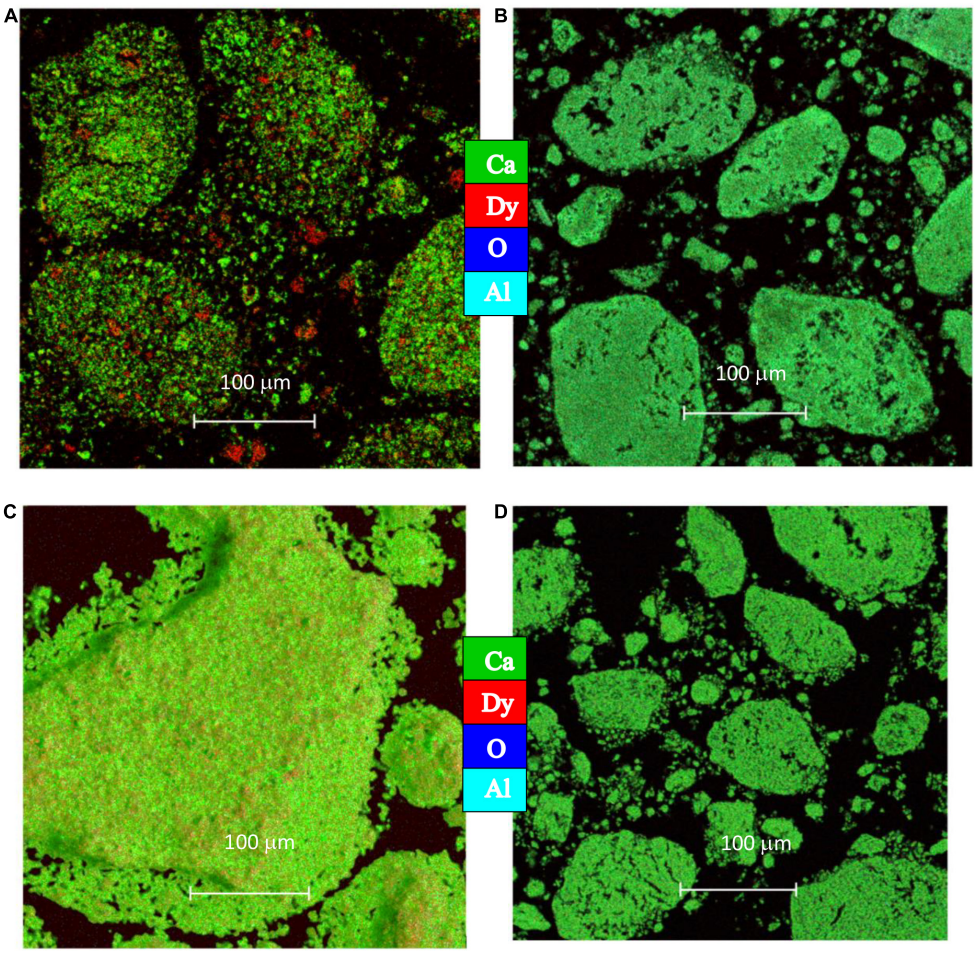

FIGURE 7 | EDS mapping for **(A)** P-CaDy20 as synthesized **(B)** P-CaDy-Al20 as synthesized, **(C)** PCaDy20 after 40 cycles **(D)** P-CaDy-Al20 after 40 cycles.

TABLE 5 | BET and BJH analysis results, as synthesized and after 40 cycles.

Material	BET surface area ($m^2\ g^{-1}$)	BJH cumulative pore volume ($cm^3\ g^{-1}$)	BJH average pore width (nm)
P-CaO	11.2	0.079	22.3
P-CaO-c	0.6	–	–
P-CaO-Al20	6.7	0.042	25.1
P-CaDy20	8.2	0.052	23.8
P-CaDy20-c	4.1	0.011	10.1
P-CaDy-Al20	13.4	0.12	41.5
P-CaDy-Al20-c	10.1	0.044	19.2

an inert support with unchanging volume, sorbent expansion during carbonation will be decreased, keeping pores open for CO_2 diffusion through the product layer (Jing et al., 2017).

Both explanations can potentially explain the improved performance of P-CaDy-Al20. TEM imaging reveals greater pore volume in P-CaDy-Al20 compared to P-CaDy20 (**Figures 6d–f**), which is also retained after cycling. EDS mapping also shows evidence of the mitigation of sintering in P-CaDy-Al20 as opposed to P-CaDy20 (**Figure 7**). The light blue aluminate domains throughout the material and around the grain boundaries could be indicative of the "pinning" effect of calcium aluminate.

Heat Storage Capacity and Comparison With Other TCES Materials

The heat storage capacities of the synthesized materials were evaluated using DSC analysis during thermal cycling and compared with experimental data from literature (see **Table 5**). **Figure 8** shows the variation of heat storage capacity with cycling, with **Figure 8A** showing that stable readings were obtained for P-CaDy-Al20. While the heat storage capacity of P-CaO-Al20 is initially higher due to the slightly higher amount of active CaO in P-CaO-Al20 (cf., **Table 1**), P-CaDy-Al20 exhibits a greater stability measured with cycling for both endothermic and exothermic processes (cf., **Figure 3**). After 40 cycles, the heat storage capacity of P-CaDy-Al20 is 25% greater than P-CaO-Al20 without Dy_2O_3. The greater exothermic heat flows in P-CaDy-Al20 are due to enhanced stability and are linked directly to enhanced carbonation conversion with cycling (cf., **Figure 3**). Cycling of pure Dy_2O_3 ascertained that the material does not act as a CO_2 sorbent, and without the inert support calcium aluminate (as in P-CaDy20; cf., **Figure 8B**), the material is unstable. However, the synergistic combination of Dy_2O_3 and $Ca_3Al_2O_6$ as inert supports achieves excellent results.

Table 5 compares the experimental results to heat storage capacities of other materials in published literature except for CuO (Alonso et al., 2015) and commercial $CaCO_3$, for which the values have been obtained using thermochemical data. P-CaDy-Al20 and P-CaO-Al20 achieve the highest heat of reaction values, even after 40 reaction cycles. Pure $CaCO_3$ has a calcination heat of reaction of 1624.6 kJ kg^{-1} [according to simulations performed using HSC Chemistry 8 ® (Roine, 2018)], but this is predicted to drop to 81 kJ kg^{-1} after 40 cycles, taking into account loss of reactivity using a sintering model (see section "Sintering Model"). As compared with other well-investigated thermochemical systems, such as Co_3O_4/CoO (Carrillo et al., 2014), BaO (Fahim and Ford, 1983), CuO (Alonso et al., 2015), Mn_2O_3/Mn_3O_4 (Carrillo et al., 2014), $(Mn_{0.1}Fe_{0.9})_2O_3$ (Carrillo et al., 2015), the spinel $(Mn_{0.33}Fe_{0.67})_2O_3$ (Al-Shankiti et al., 2019; Hamidi et al., 2019), $(Co_{0.867}Fe_{0.133})_3O_4$ (Block et al., 2014), and $(Co_{0.99}Mn_{0.01})_3O_4$ (Carrillo et al., 2014), P-CaDy-Al20 has the largest exothermic heat storage capacity after a longer cycling period. After 40 cycles, this heat of reaction (582.2 kJ kg^{-1}) is 3.3 times greater than $(Mn_{0.33}Fe_{0.67})_2O_3$ (Hamidi et al., 2019), 18% higher than the well-known Co_3O_4/CoO redox pair (Carrillo et al., 2014) and 7.3 times higher than Mn_2O_3/Mn_3O_4 (Carrillo et al., 2014). Therefore, it can be concluded that

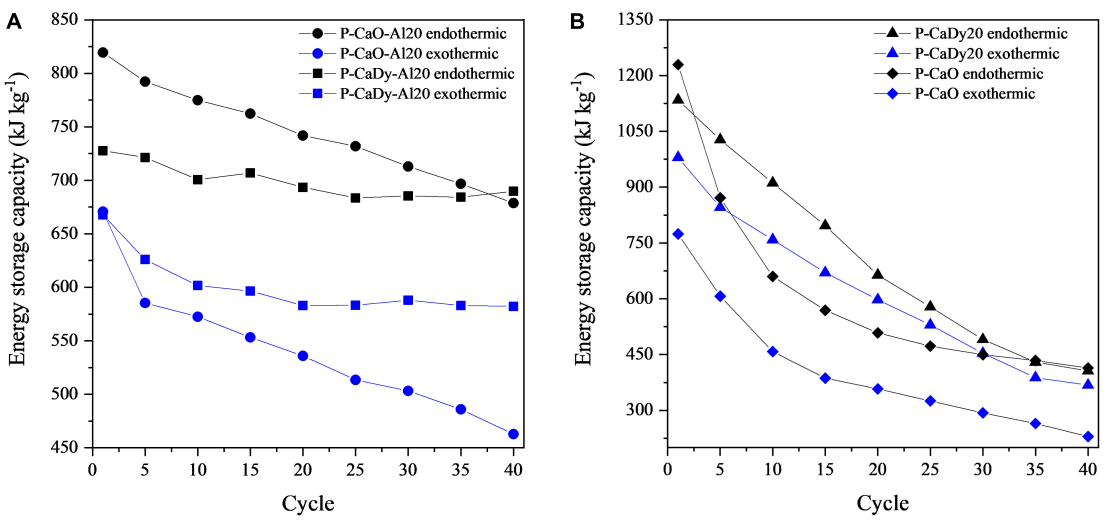

FIGURE 8 | (A) Endothermic and exothermic heat flows for supported and **(B)** weight loss of supported materials under CO_2.

the materials P-CaDy-Al20 and P-CaO-Al20 have the best performance so far found in literature for this type of small laboratory scale analysis. Further work should be perfomed at reactor level to compare the materials in this work with reactor-scale tests in published literature (Tescari et al., 2013).

Feasibility Study

Figures 9A,B show the application of sintering models to the first 40 carbonation cycles of experimental data (cf., sections "Material Characterization" and "Calcination-Carbonation Cycling Analysis"). Using the sintering model with the greatest accuracy (**Table 6**), the long-term performance of selected synthesized materials was modeled (**Figure 9C**).

A feasibility assessment of the selected synthesized materials and commercial $CaCO_3$ is presented in **Table 6**. The indicated sintering models were used to determine the number of cycles for carbonation conversion to fall below 20%. This cut-off has been suggested as the minimum carbonation conversion capacity to allow for optimum plant efficiency using a pressurized fluidized bed combustor as the carbonator (Prieto et al., 2016). If carbonation conversion drops below this capacity, it will need to be replaced with fresh material.

The sintering models determine that residual carbonation conversion does not drop below 20% for P-CaDy-Al20, even after 30 years of continuous cycling, whereas unsupported P-CaO would need to be replaced after seven cycles and Comm-$CaCO_3$ would need to be replaced every six cycles. This would incur

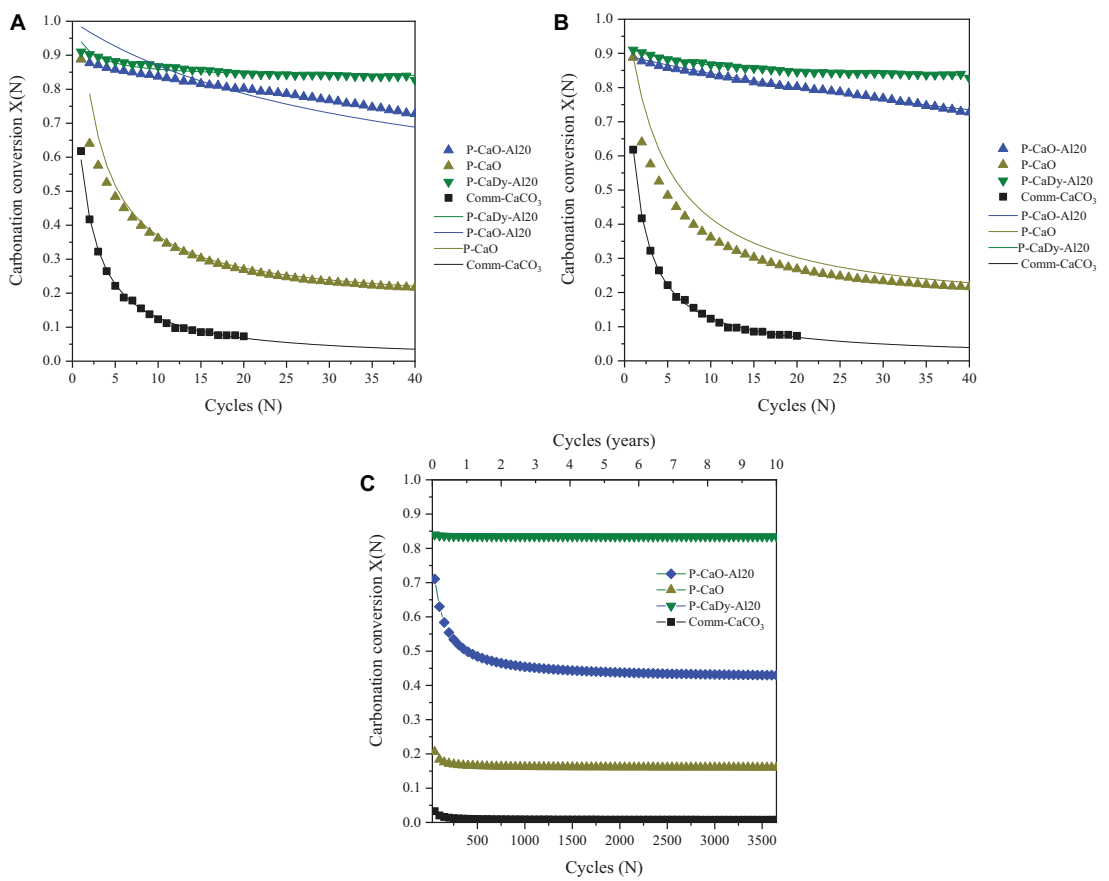

FIGURE 9 | Sintering model compared to experimental data using **(A)** deactivation sintering model (Luo et al., 2010) and **(B)** semi-empirical model (Hu et al., 2016), with **(C)** long-term CaO-based sorbent performance using best fitting sintering models.

TABLE 6 | Feasibility assessment of selected candidate materials.

Material	Sintering model	Cycles to drop below 20% conversion (days)	Number of sorbent replacements needed after 30 years of cycling	μStorage after 40 cycles (kg kWh^{-1})	μStorage after 30 years of cycling assuming 1 cycle per day (kg kWh^{-1})
P-CaO	[53]	7	1564	15.7	24533
P-CaO-Al20	[55]	58	189	7.78	1470
P-CaDy-Al20	[53]	Infinite	None (1)	6.18	6.18
Comm-$CaCO_3$	[55]	6	1825	44.3	80911

additional operation and maintenance costs on top of the cost required to replace the material.

When evaluating the mass specific storage utilization ($\mu_{Storage}$) after 40 charge and discharge cycles, the best performing materials are P-CaDy-Al20 and P-CaO-Al20, with storage densities of 6.2 and 7.8 kg kWh^{-1}, respectively. When considering the amount of material required after replacement over the CSP plant lifetime, the improved storage utilization of P-CaDy-Al20 is even more apparent. After 30 years, it is expected to retain a storage utilization (μstorage) as low as 6.2 kg kWh^{-1}, compared to 81 tons kWh^{-1} for commercial $CaCO_3$ (**Table 6**). This is due to its superior stability and extremely high residual carbonation conversion. These results justify the additional cost of inert supports for the synthesized material P-CaDy-Al20 and indicate its suitability for large-scale energy storage applications.

CONCLUSION

A CaO-based material supported with $Ca_3Al_2O_6$ and Dy_2O_3 shows excellent energy sorption cycling under a CO_2 atmosphere. The main benefits are due to its retention of high surface area compared to CaO and the addition of anti-sintering properties, even under an atmosphere which accelerates sintering. A conversion capacity of 82.7% is retained after 40 cycles under severe calcination conditions while other materials in the literature show high deactivation. The retention of conversion capacity is not the only feature that makes the material promising for TCES. A further feasibility study found that the exothermic heat of reaction obtained (582.2 kJ kg^{-1}) is up to seven times higher than other TCES systems (like Mn_2O_3/Mn_3O_4 redox cycle). In addition, a sintering model was applied to evaluate the specific storage utilization. In this study it was found that 6.2 kg kWh^{-1} is required for the CaO supported with $Ca_3Al_2O_6$ and Dy_2O_3, while for commercial limestone 81 tons kWh^{-1} will be needed over 30 years (a common CSP plant life). This is because the conversion capacity of commercial limestone drops below 20% after six thermal cycles (or 6 days assuming one cycle per day) and this implies the need for 1825 replacements over a common CSP plant life. This initial feasibility study shows that despite the additional cost of the supports, their addition is beneficial for the stable and long-term performance of the storage system.

DATA AVAILABILITY STATEMENT

The raw data supporting the conclusions of this article will be made available by the authors, without undue reservation.

AUTHOR CONTRIBUTIONS

LF-H, AB, and SD contributed to conception and design of the study. AB and SD obtained funding for the research. LF-H and XG performed the experiments. AT, AB, and SD supervised the experimental results. All authors contributed to the writing the manuscript, manuscript revision, read, and approved the submitted version.

FUNDING

This research was performed as part of the Australian Solar Thermal Research Initiative (ASTRI), a project supported by the Australian Government, through the Australian Renewable Energy Agency (ARENA).

REFERENCES

Aihara, M., Nagai, T., Matsushita, J., Negishi, Y., and Ohya, H., (2001). Development of porous solid reactant for thermal-energy storage and temperature upgrade using carbonation/decarbonation reaction. *Appl. Energy* 2001, 225–238. doi: 10.1016/s0306-2619(00)00072-6

Albrecht, K. O., Wagenbach, K. S., Satrio, J. A., Shanks B. H., and Wheelock, T. D. (2008). Development of a CaO-Based CO2 Sorbent with Improved Cyclic Stability. *Industr. Eng. Chem. Res.* 47, 7841–7848. doi: 10.1021/ie8007743

Alonso, E., Rabago, C. P., Licurgo, J., Fuentealba, E., and Estrada, C. A. (2015). First experimental studies of solar redox reactions of copper oxides for thermochemical energy storage. *Sol Energy* 115, 297–305. doi: 10.1016/j.solener.2015.03.005

Al-Shankiti, I. A., Ehrhart, B. D., Ward, B. J., Bayon, A., Wallace, M. A., Bader, R., et al., (2019). Particle design and oxidation kinetics of iron-manganese oxide redox materials for thermochemical energy storage. *Sol. Energy* 183, 17–29. doi: 10.1016/j.solener.2019.02.071

André, L., Abanades S., and Flamant, S. (2016). Screening of thermochemical systems based on solid-gas reversible reactions for high temperature solar thermal energy storage. *Renew. Sustain. Energy Rev* 64, 703–715. doi: 10.1016/j.rser.2016.06.043

André, L., and Abanades, S. (2018). Investigation of metal oxides, mixed oxides, perovskites and alkaline earth carbonates/hydroxides as suitable candidate materials for high-temperature thermochemical energy storage using reversible solid-gas reactions. *Mater. Today Energy* 10, 48–61. doi: 10.1016/j.mtener.2018.08.007

Angeli, S. D., Martavaltzi C. S. and Lemonidou, A. A. (2014). Development of a novel-synthesized Ca-based CO2 sorbent for multicycle operation: parametric study of sorption. *Fuel* 127, 62–69. doi: 10.1016/j.fuel.2013.10.046

Awan, AB., Zubair, M., Praveen, R. P., and Bhatti, A. R. (2019). Design and comparative analysis of photovoltaic and parabolic trough based CSP plants. *Sol. Energy* 183, 551–565. doi: 10.1016/j.solener.2019.03.037

Azimi, B., Tahmasebpoor, M., Sanchez-Jimenez, P. E., Perejon, A., and Valverde, J. M. (2019). Multicycle CO2 capture activity and fluidizability of Al-based synthesized CaO sorbents. *Chem. Eng. J.* 358, 679–690. doi: 10.1016/j.cej.2018.10.061

Bayon, A., Bader, R., Jafarian, M., Fedunik-Hofman, L., Sun, Y., Hinkley, J., et al. (2018). Techno-economic assessment of solid-gas thermochemical energy storage systems for solar thermal power applications. *Energy* 149, 473–484. doi: 10.1016/j.energy.2017.11.084

Benitez-Guerrero, M., Sarrion, B., Perejon, A., Sanchez-Jimenez, P. E., and Perez-Maqueda, L. A., and Valverde, J. M. (2017). Large-scale high-temperature solar energy storage using natural minerals. *Sol. Energy Mater. Sol. Cells* 168, 14–21. doi: 10.1016/j.solmat.2017.04.013

Benitez-Guerrero, M., Valverde, J. M., Perejon, A., Sanchez-Jimenez, P. E., and Perez-Maqueda, L. A., (2018). Low-cost Ca-based composites synthesized by biotemplate method for thermochemical energy storage of concentrated solar power. *Appl. Energy* 210, 108–116. doi: 10.1016/j.apenergy.2017.10.109

Block, T., Knoblauch, N., and Schmücker, M. (2014). The cobalt-oxide/iron-oxide binary system for use as high temperature thermochemical energy storage material. *Thermochim. Acta* 577, 25–32. doi: 10.1016/j.tca.2013.11.025

Broda, M., Kierzkowska, A. M., and Müller, C. R. (2012). Influence of the Calcination and Carbonation Conditions on the CO2 Uptake of Synthetic Ca-Based CO2 Sorbents. *Environ. Sci. Technol* 46, 10849–10856. doi: 10.1021/es302757e

Calle, A. D. L., Bayon A., and Too, Y. C. S. (2018). Impact of ambient temperature on supercritical CO2 recompression Brayton cycle in arid locations: finding the optimal design conditions. *Energy* 153, 1016–1027. doi: 10.1016/j.energy.2018.04.019

Carrillo, A. J., David Serrano, P., Pizarro, P., and Coronado, J. M. (2015). Improving the Thermochemical Energy Storage Performance of the Mn2O3/Mn3O4 Redox Couple by the Incorporation of Iron. *ChemSusChem*. 8, 1947–1954. doi: 10.1002/cssc.201500148

Carrillo, A. J., Moya, J., Sandoval, A. B., Jana, P., O'Shea, V. A. D. L. P., Romero, M., et al., (2014). Thermochemical energy storage at high temperature via redox cycles of Mn and Co oxides: pure oxides versus mixed ones. *Sol. Energy Mater. Sol. Cells* 123, 47–57. doi: 10.1016/j.solmat.2013.12.018

Chacartegui, R., Alovisio, A., Ortiz, C., Valverde, J. M., Verda, V., and Becerra, J. A., (2016). Thermochemical energy storage of concentrated solar power by integration of the calcium looping process and a CO2 power cycle. *Appl. Energy* 173, 589–605. doi: 10.1016/j.apenergy.2016.04.053

Cotton, F. A., Wilkinson, G., Murillo, C. A., and Bochmann, M. (1999). *Advanced Inorganic Chemistry*. 6th ed. New York: Wiley-Interscience.

Degen, T., Sadki, M., Bron, E., König, U., and Nénert, G. (2014). HighScore Plus, in *Powder Diffraction* United Kingdom: Malvern Panalytical Instrumentation compan

Derevschikov, V. S., Lysikov A. I., and Okunev, A. G. (2011). High Temperature CaO/Y2O3 Carbon Dioxide Absorbent with Enhanced Stability for Sorption-Enhanced Reforming Applications. *Industr. Eng. Chem. Res.* 50, 12741–12749. doi: 10.1021/ie2015334

Edwards, S., and Materić, V. (2012). Calcium looping in solar power generation plants. *Sol. Energy* 86, 2494–2503. doi: 10.1016/j.solener.2012.05.019

Erans, M., Jeremias, M., Zheng, L., Joseph Y. G., Blamey, J., Manovic, V., et al., (2018). Pilot testing of enhanced sorbents for calcium looping with cement production. Applied Energy, 225, 392–401. doi: 10.1016/j.apenergy.2018.05.039

Fahim M. A. and Ford, J. D. (1983). Energy storage using the BaO2-BaO reaction cycle. *The Chem. Eng. J*. 1983. 27, 21–28. doi: 10.1016/0300-9467(83)80042-2

Gil, A., Medrano, M., Martorell, I., Lázaro, A., Dolado, P., Zalba, B. et al. (2010). State of the art on high temperature thermal energy storage for power generation. Part 1—Concepts, materials and modellization. *Renew. Sustain. Energy Rev.* 14, 31–55. doi: 10.1016/j.rser.2009.07.035

Grasa, G. S., Abanades, J. C., Alonso, M., and González, B. (2008). Reactivity of highly cycled particles of CaO in a carbonation/calcination loop. *Chem. Eng. J.* 137, 5615–5667.

Grasa, G. S., and Abanades, J. C. (2006). CO2 Capture Capacity of CaO in Long Series of Carbonation/Calcination Cycles. *Industr. Eng. Chem. Res* 45, 8846–8851. doi: 10.1021/ie0606946

Greenblatt, H. B., Brown, N. R., Slaybaugh, R., Wilks, T., Stewart, E., and McCoy, S. T. (2017). The Future of Low-Carbon Electricity. *Ann. Rev Environ. Resour.* 42, 289–316.

Hamidi, M., Bayon, A., Wheeler, V. M., Kreider, P., Wallace, M. A., Tsuzuki, T., et al., (2019). Reduction kinetics for large spherical 2:1 iron–manganese oxide redox materials for thermochemical energy storage. *Chem. Eng. Sci.* 201, 74–81. doi: 10.1016/j.ces.2019.02.012

Hu, Y. C., Liu, W. Q., Sun, J., Li, M. K., Yang, X. W., Zhang, Y., et al., (2015). Incorporation of CaO into novel Nd2O3 inert solid support for high temperature CO2 capture. *Chem. Eng. J.* 273, 333–343. doi: 10.1016/j.cej.2015.03.074

Hu, Y., Liu, W., Sun, J., Yang, X., Zhou, Z., Zhang Y., et al., (2016). High Temperature CO2 Capture on Novel Yb2O3-Supported CaO-Based Sorbents. *Energy Fuels* 30, 6606–6613. doi: 10.1021/acs.energyfuels.6b01185

Jana, P., O'Shea, V. A. D. L. P., Coronado, J. M., and Serrano, D. P. (2010). Cobalt based catalysts prepared by Pechini method for CO2-free hydrogen production by methane decomposition. *Int. J. Hydrogen Energy* 35, 10285–10294. doi: 10.1016/j.ijhydene.2010.07.125

Jing, J., Li, T., Zhang, X., Wang, S., Feng, J., Turmel, W. A., et al., (2017). Enhanced CO2 sorption performance of CaO/Ca3Al2O6 sorbents and its sintering-resistance mechanism. *Appl. Energy* 199, 225–233. doi: 10.1016/j.apenergy.2017.03.131

Kierzkowska, A. M., Pacciani, R., and Müller, C. R. (2013). CaO-based CO2 sorbents: from fundamentals to the development of new, highly effective materials. *ChemSusChem*. 6, 1130–1148. doi: 10.1002/cssc.201300178

Li, C., Wu U. -T and Lin, H. -P., (2014). Cyclic performance of CaCO3@mSiO2 for CO2 capture in a calcium looping cycle. *J. Mater. Chem. A* 2, 8252–8257. doi: 10.1039/c4ta00516c

Li, Y., Shi, L., Liu, C., He, Z., Wu, S. (2015). Studies on CO2 uptake by CaO/Ca3Al2O6 sorbent in calcium looping cycles. *J. Therm. Anal. Calorim*, 120, 1519–1528. doi: 10.1007/s10973-015-4480-9

Li, Z. -S., Cai, N. -S., Huang Y. -Y., and Han, H. J. (2005). Synthesis, experimental studies, and analysis of a new calcium-based carbon dioxide absorbent. *Energy Fuels* 19, 1447–1452.

Li, Z., Liu Y., and Cai, N. (2013). Understanding the effect of inert support on the reactivity stabilization for synthetic calcium based sorbents. *Chem. Eng. Sci.* 89, 235–243. doi: 10.1016/j.ces.2012.12.006

Liu, M., Tay, N. H. S., Bell, S., Belusko, M., Jacob, R., Will, G., et al. (2016). Review on concentrating solar power plants and new developments in high temperature thermal energy storage technologies. *Renew Sustain. Energy Rev.* 53, 1411–1432. doi: 10.1016/j.rser.2015.09.026

Liu, W., An, H., Qin, C., Yin, J., Wang, G., Feng, B., et al., (2012b). Performance enhancement of calcium oxide sorbents for cyclic CO2 capture: a review. *Energy Fuels* 26, 2751–2767. doi: 10.1021/ef300220x

Liu, W., González, B., Dunstan, M. T., Sultan, D. S., Pavan, A., Ling, C. D., et al., (2016). Structural evolution in synthetic, Ca-based sorbents for carbon capture. *Chemical Eng. Science* 139, 15–26. doi: 10.1016/j.ces.2015.09.016

Liu, W., Dennis, J. S., Sultan, D. S., Redfern, S. A. T., and Scott, S. A. (2012a)An investigation of the kinetics of CO2 uptake by a synthetic calcium based sorbent. *Chem. Eng. Sci.*, 69, 644–658. doi: 10.1016/j.ces.2011.11.036

Lu S., and Wu, S., (2016). Calcination–carbonation durability of nano CaCO3 doped with Li2SO4. *Chem. Eng. J.* 294, 22–29. doi: 10.1016/j.cej.2016.02.100

Lu, H., Khan, A., Pratsinis S. E. and Smirniotis, P. G. (2009). Flame-Made Durable Doped-CaO Nanosorbents for CO2 Capture. *Energy Fuels* 23, 1093–1100. doi: 10.1021/ef8007882

Luo, C., Zheng, Y., Ding, N., Wu, Q., Bian G., and Zheng, C. (2010). Development and Performance of CaO/La2O3 Sorbents during Calcium Looping Cycles for CO2 Capture. *Industr. Eng. Chem. Res.* 49, 11778–11784.

Manovic, V., and Anthony, E. J., (2005). Thermal Activation of CaO-Based Sorbent and Self-Reactivation during CO2 Capture Looping Cycles. *Environ. Sci. Technol.* 42, 4170–4174. doi: 10.1021/es800152s

Ortiz, C., Romano, M. C., Valverde, J. M., Binotti, M., and Chacartegui, R., (2018a). Process integration of Calcium-Looping thermochemical energy storage system in concentrating solar power plants. *Energy* 155, 535–551. doi: 10.1016/j.energy.2018.04.180

Ortiz, C., Valverde, J. M., Chacartegui R., and Perez-Maqueda, L. A. (2018b). Carbonation of Limestone Derived CaO for Thermochemical Energy Storage: from Kinetics to Process Integration in Concentrating Solar Plants. *ACS Sustain. Chem. Eng.* 6, 6404–6417. doi: 10.1021/acssuschemeng.8b00199

Peng, W., Xu, Z., Luo, C., and Zhao, H. (2015). Tailor-Made Core–Shell CaO/TiO2–Al2O3 Architecture as a High-Capacity and Long-Life CO2 Sorbent. *Environ. Sci. Technol* 49, 8237–8245. doi: 10.1021/acs.est.5b01415

Perry, D. L. (2015). *Handbook of Inorganic Compounds*. CRC Press. United States.

Ping, H., Wang Y. and Wu, S. (2016). Preparation of MgO-coated nano CaO using adsorption phase reaction technique for CO2 sorption. *RSC Adv.* 6, 41239–41246. doi: 10.1039/c6ra05452h

Prieto, C., Cooper, P., Fernández, A. I., Cabeza, L. F. (2016). Review of technology: thermochemical energy storage for concentrated solar power plants. *Renew. Sustain. Energy Rev.* 60, 909–929. doi: 10.1016/j.rser.2015.12.364

Qin, C., Du, H., Liu, L., Yin J., and Feng, B. (2014). CO2 Capture Performance and Attrition Property of CaO-Based Pellets Manufactured from Organometallic Calcium Precursors by Extrusion. *Energy Fuels* 28, 329–339. doi: 10.1021/ef4012609

Radfarnia H. R. and Sayari, A. (2015). A highly efficient CaO-based CO2 sorbent prepared by a citrate-assisted sol-gel technique. *Chem. Eng. J.* 262, 913–920. doi: 10.1016/j.cej.2014.09.074

Roine, Q. A., (2018). HSC Chemistry 8 0. Outotec, Pori

Sanchez-Jimenez, P. E., Perez-Maqueda, L. A. and Valverde, J. M., (2014). Nanosilica supported CaO: a regenerable and mechanically hard CO2 sorbent at Ca-looping conditions. *Appl. Energy* 118, 92–99. doi: 10.1016/j.apenergy.2013.12.024

Sarrión, B., Perejón, A., Sánchez-Jiménez, P. E., Pérez-Maqueda, L. A., and Valverde, J. M. (2018). Role of calcium looping conditions on the performance of natural and synthetic Ca-based materials for energy storage. *J. CO2 Util.* 28, 374–384. doi: 10.1016/j.jcou.2018.10.018

Schaube, F., Wörner A., and Tamme, R., (2011). High temperature thermochemical heat storage for concentrated solar power using gas–solid reactions. *J. Sol. Energy Eng.* 133, 31006.

Stanmore, B. R., and Gilot, P., (2005). Review: calcination and carbonation of limestone during thermal cycling for CO2 sequestration. *Fuel Proce. Technol.* 86, 1707–1743. doi: 10.1016/j.fuproc.2005.01.023

Starke, A. R., Cardemil, J. M., Escobar, R., and Colle, S. (2018). Multi-objective optimization of hybrid CSP+PV system using genetic algorithm. *Energy* 147, 490–503. doi: 10.1016/j.energy.2017.12.116

Steinhagen, H. M., and Nitsch, J. (2005). The Contribution of Renewable Energies to a Sustainable Energy Economy. *Process Safety Environ. Prot.*, 83, 285–297. doi: 10.1205/psep.05084

Stone, F. S. (1960). Reactivity of Solids. in 4th International Symposium on the Reactivity of Solids. Amsterdam: Elsevier. doi: 10.1016/0168-7336(88)80069-x

Sun, J., Liu, W., Li, M., Yang, X., Wang, W., Hu, Y., et al., (2016). Mechanical Modification of Naturally Occurring Limestone for High-Temperature CO2 Capture. *Energy Fuels* 8, 6597–6605. doi: 10.1021/acs.energyfuels.6b01131

Tescari, S., Neises, M., de Oliveira, L., Sattler, C., and Neveu, P. (2013). Thermal model for the optimization of a solar rotary kiln to be used as high temperature thermochemical reactor. *Sol. Energy* 95, 279–289. doi: 10.1016/j.solener.2013.06.021

Valverde, J. M. (2013). Ca-based synthetic materials with enhanced CO2 capture efficiency. *J. Mater. Chem. A* 1, 447–468. doi: 10.1039/c2ta00096b

Valverde, J. S., -López, M. B., Perejón, A., Sánchez-Jiménez P. E., and Pérez-Maqueda, L. A. (2017). Effect of Thermal Pretreatment and Nanosilica Addition on Limestone Performance at Calcium-Looping Conditions for Thermochemical Energy Storage of Concentrated Solar Power. *Energy Fuels* 31, 4226–4236. doi: 10.1021/acs.energyfuels.6b03364

Wang, N., Feng, Y., Liu, L., and Guo, X. (2018). Effects of preparation methods on the structure and property of Al-stabilized CaO-based sorbents for CO2 capture. *Fuel Process. Technol.* 173, 276–284. doi: 10.1016/j.fuproc.2018.02.005

Zhao, M., Shi, J., Zhong, X., Tian, S., Blamey, J., Jiang J., et al., (2014). A novel calcium looping absorbent incorporated with polymorphic spacers for hydrogen production and CO2 capture. *Energy Environ. Sci.* 7, 3291–3295. doi: 10.1039/c4ee01281j

Zhou, Z., Qi, Y., Xie, M., Cheng, Z., and Yuan, W. (2012). Synthesis of CaO-based sorbents through incorporation of alumina/aluminate and their CO2 capture performance. *Chem. Eng. Sci.* 74, 172–180. doi: 10.1016/j.ces.2012.02.042

Zhou, Z., Xu, P., Xie, M., Cheng, Z., and Yuan, W. (2013)Modeling of the carbonation kinetics of a synthetic CaO-based sorbent. *Chemical Engineering Science*, 95, 283–290. doi: 10.1016/j.ces.2013.03.047

Conflict of Interest: The authors declare that the research was conducted in the absence of any commercial or financial relationships that could be construed as a potential conflict of interest.

NOMENCLATURE

ΔH_r, Reaction enthalpy, kJ mol^{-1};
k, Deactivation constant, min^{-1};
M, Molar mass, g mol^{-1};
m_i, Initial sample mass, g;
m(t), Sample mass after t min of carbonation, g;
$m_{X=1}$, Theoretical sample mass after 100% conversion, g;
T, Temperature, K;
X(N), Carbonation conversion after N cycles;
X_r, Residual carbonation conversion;
X(t), Carbonation conversion after t time;
$X(t)_{Eff}$, Effective carbonation conversion (considering inert support) after t time;
$\mu_{Storage}$, Gravimetric energy storage utilization, kg kWh^{-1}.